

**Anisotropy of magnetoelastic properties in epitaxial  $\text{Co}_2\text{Fe}_x\text{Mn}_{1-x}\text{Si}$  Heusler alloy thin films**A. Nabiałek<sup>1</sup>, O. Chumak<sup>1</sup>, A. Lynnyk<sup>1</sup>, J. Z. Domagała<sup>1</sup>, A. Pacewicz<sup>2</sup>, B. Salski<sup>2</sup>, J. Krupka<sup>3</sup>, T. Yamamoto<sup>4</sup>, T. Seki<sup>4,5</sup>, K. Takanaishi<sup>4,5,6,\*</sup>, L. T. Baczewski<sup>1</sup> and H. Szymczak<sup>1</sup><sup>1</sup>*Institute of Physics, Polish Academy of Sciences, Al. Lotników 32/46, 02-668 Warsaw, Poland*<sup>2</sup>*Institute of Radioelectronics and Multimedia Technology, Warsaw University of Technology, Nowowiejska 15/19, 00-665 Warsaw, Poland*<sup>3</sup>*Institute of Microelectronics and Optoelectronics, Warsaw University of Technology, 00 662 Warsaw, Poland*<sup>4</sup>*Institute for Materials Research, Tohoku University, Sendai 980-8577, Japan*<sup>5</sup>*Center for Spintronics Research Network, Tohoku University, Sendai 980-8577, Japan*<sup>6</sup>*Center for Science and Innovation in Spintronics, Core Research Cluster, Tohoku University, Sendai 90-8577, Japan*

(Received 6 April 2022; revised 14 June 2022; accepted 30 June 2022; published 2 August 2022)

A strain modulated ferromagnetic resonance technique was applied to determine two cubic magnetoelastic constants of the epitaxially grown 30-nm-thick  $\text{Co}_2\text{Fe}_x\text{Mn}_{1-x}\text{Si}$  magnetic layers with different Fe and Mn contents, which were deposited on a MgO substrate with a 20-nm-thick Cr buffer layer—MgO (001) || Cr(001) ||  $\text{Co}_2\text{Fe}_x\text{Mn}_{1-x}\text{Si}$  (001). It was found that, for the samples with the Fe content  $x = 0.4$  or higher, the magnitudes of the two cubic magnetoelastic constants are clearly different, showing that the magnetoelastic properties of these samples are different than in the case of isotropic samples for which these two constants are expected to be equal. The magnitude of the cubic magnetocrystalline anisotropy constant reveals an evident maximum at the composition of  $x = 0.4$ , which corresponds to the minimum of the minor spin density of states, and thus the correlation between the cubic magnetocrystalline anisotropy and the electronic band structure. For all the investigated samples, a large perpendicular component of the magnetocrystalline anisotropy was observed as well as inhomogeneous broadening of the ferromagnetic resonance linewidth.

DOI: [10.1103/PhysRevB.106.054406](https://doi.org/10.1103/PhysRevB.106.054406)**I. INTRODUCTION**

Thanks to the low density of states at the Fermi level for the minority-spin channel, the half-metallic  $\text{Co}_2$ -based Heusler alloys reveal high spin polarization, and thus they are promising materials for applications in spintronics [1]. In the case of  $\text{Co}_2\text{Fe}_x\text{Mn}_{1-x}\text{Si}$  compounds, the Fermi energy falls close to the middle of the gap in the minority states for intermediate Fe concentration. The magnetic and electronic properties of such compounds are very stable against external influences, which will not be able to change the number of minority electrons [2]. In particular, the  $\text{Co}_2\text{Fe}_{0.4}\text{Mn}_{0.6}\text{Si}$  (CFMS) composition was intensively studied for practical applications, among others in vortex spin-torque oscillators [3]. In such applications, low magnetic attenuation at microwave frequencies is also desirable. The ultrafast demagnetization and the intrinsic Gilbert damping in the  $\text{Co}_2$ -based Heusler alloys were investigated by several researchers [4–6]. Fortunately, among the  $\text{Co}_2\text{Fe}_x\text{Mn}_{1-x}\text{Si}$  series, the composition with  $x = 0.4$  reveals also the lowest magnetic damping, with a Gilbert damping factor of about  $3.5 \times 10^{-3}$ , for the samples with magnetic layer thickness of 30 nm [6]. In previous work [6] the ultrafast demagnetization mechanism in a series of  $\text{Co}_2\text{Fe}_x\text{Mn}_{1-x}\text{Si}$  films was shown to be correlated with the band structure of the investigated alloys, i.e., with the spin

density of states at the Fermi level. In the present study the same series of the samples were used to determine the magnetoelastic (ME) properties as well as the magnetocrystalline (MC) anisotropy.

ME properties of the Heusler alloys remain poorly researched. In particular, to the best knowledge of the authors, experimental investigations of the ME properties of  $\text{Co}_2\text{Fe}_x\text{Mn}_{1-x}\text{Si}$  series with changing Fe content have not been performed so far. In our previous papers [7,8] ME properties of the CFMS thin films only for the composition with  $x = 0.4$  were investigated as a function of thickness. In all series of the samples, an increase of the ME constants magnitudes with increasing thickness of magnetic layer (in the range 15–50 nm) was observed. In Ref. [8] the Gilbert damping factor was also investigated. It was found that, for the films for which the spin pumping phenomenon can be neglected, the Gilbert damping factor also increases with increasing thickness of the magnetic layer. Such changes of ME constants and Gilbert damping factor may suggest a correlation between both parameters. However, an increase of Gilbert damping with increasing thickness of the magnetic layer can be also correlated with the eddy currents induced in conducting magnetic layers [9]. Generally it is expected that stronger ME effect should result in stronger damping. However, the quantitative correlation between these two phenomena is complicated. The up-to-date developed models assume correlation of the magnetic damping with the strain fluctuations induced by the ME effect [10]. On the other hand, materials characterized by strong ME coupling and low damping are also available [11].

\*Present address: Advanced Science Research Center (ASRC), Japan Atomic Energy Agency (JAEA), Tokai, Ibaraki 319-1195, Japan.

To determine the ME properties one can either measure the magnetostriction, i.e., the changes of the sample dimensions in external magnetic field, which can be done using different kinds of dilatometers or diffraction (x-ray, neutron) methods, or apply one of the indirect methods based, e.g., on Villari or Wiedemann effects [12]. Strain modulated ferromagnetic resonance (SMFMR) is one of an indirect method, which enables determination of the ME properties of the magnetic thin films [13,14]. To determine ME properties of thin films, only a few method can be applied. Among other methods of testing the ME properties of thin films, one can also mention the strain gauge [15], or small-angle-magnetization-rotation method [16]. In the SMFMR method, a periodic strain in a magnetic sample is induced. Application of the phase-sensitive detection enables the determination of the shift of the FMR line even for very small strain amplitudes. In other methods to modify the magnetic properties, a large static strain can be also applied [17,18]. In our previous works [7,8], we used the SMFMR method to determine only one isotropic ME constant for each sample. However, the recent electronic structure study based on the first-principles calculation for the ME properties in  $\text{Co}_2$ -based  $\text{Co}_2\text{XAl}$  ( $X = \text{V}, \text{Ti}, \text{Cr}, \text{Mn}, \text{Fe}$ ) full Heusler compounds shows that both cubic ME constants for these compounds may differ significantly [19]. (Note that, for samples whose magnetoelastic properties isotropic both cubic ME constants  $b_1$  and  $b_2$  are expected to be equal. For the definition of the two magnetoelastic constants see Eq. (4) in Sec. IV description and their applications.) Additionally, a huge change of the ME constants is expected when Mn is replaced by Fe [19].

By using an appropriate experimental arrangement, the SMFMR technique enables determination of both ME constants for the magnetic epitaxial layers with cubic symmetry [14]. For this reason, we used this method in order to determine both cubic magnetoelastic constants for the series of the  $\text{Co}_2\text{Fe}_x\text{Mn}_{1-x}\text{Si}$  Heusler alloy thin films with different Fe and Mn contents. The aim of the present work is also to find out experimentally the correlation between the ME properties, MC anisotropy, magnetic damping and the band structure of the investigated samples.

## II. EXPERIMENTAL DETAILS

The films with the 30-nm-thick  $\text{Co}_2\text{Fe}_x\text{Mn}_{1-x}\text{Si}$  magnetic layer, in which  $x$  was set to be 0.0, 0.25, 0.4, 0.5, 0.6, 0.75, and 1.0, were deposited using ultrahigh-vacuum-compatible magnetron sputtering system. Details on the sample preparation as well as their structural characterization using *in situ* reflection high-energy electron-diffraction images, and *ex situ* x-ray diffraction (XRD) have already been reported in previous works [6,20]. The samples were grown on a MgO substrate with the 20-nm-thick Cr buffer layer to reduce the mismatch between lattice constants of MgO and of magnetic layer. The streak patterns of RHEED images for all the samples suggested that the relatively flat surfaces were formed. The mismatch between the MgO and Cr was estimated to be about 2.4% and between Cr and the magnetic layer about 1.7%—this mismatch did not change significantly with the magnetic layer composition. The magnetic layers were also covered by a 3-nm-thick Al capping layer. The XRD studies

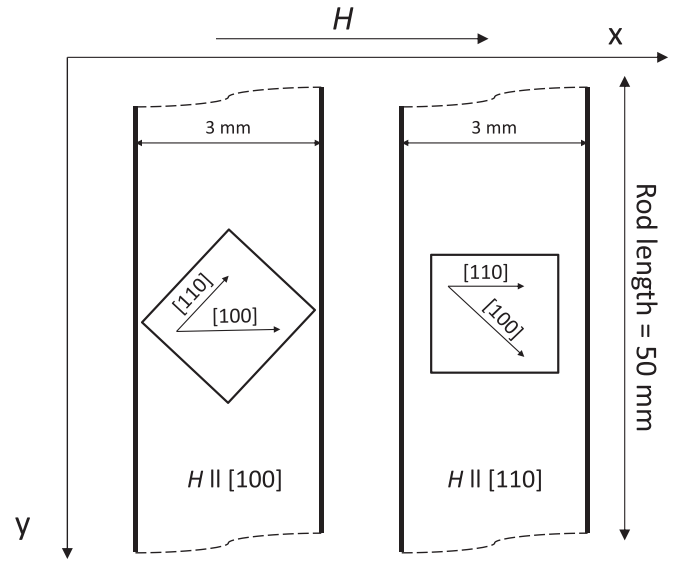


FIG. 1. The scheme of fixing the sample to the quartz rod in SMFMR experiments for the external magnetic field in-plane of the film and parallel to the [100] or [110] axis of the CFMS layer, respectively.

showed that the samples were epitaxially grown and have the cubic structure. They reveal a high (about 80%) degree of B2 ordering and moderate (about 20%) degree of L21 ordering. For all the investigated samples in this study, one of the cubic axes of the epitaxial magnetic layer was perpendicular to the surface of the film, and the other two parallel to the surface of the film. The epitaxial relationship for all the samples was as follows: the [100] axis of  $\text{Co}_2\text{Fe}_x\text{Mn}_{1-x}\text{Si}$  was parallel to the [110] axis to the MgO substrate. References [6,20] have reported also the results of studies on the in-plane magnetization hysteresis loop, as well as on the ultrafast magnetization-dynamics using the time-resolved magneto-optical Kerr effect (TRMOKE) magnetometer.

The SMFMR system used in the present experiments slightly differs from that presented in Ref. [14]. This system can be used only at room temperature, but it offers higher accuracy of the ME constants determination. The investigated samples were cut in the form of the square-shaped pieces (approximately  $2 \times 2 \text{ mm}^2$ ), and the thickness of the MgO substrate was about 0.5 mm. The surface of samples was glued to the polycrystalline quartz rod with 50 mm length and square ( $3 \times 3 \text{ mm}^2$ ) cross section, in which ultrasound (about 48 kHz) standing waves were excited using a crystalline quartz transducer attached to the one of the ends of the rod. The scheme of fixing the samples to the quartz rod is shown in Fig. 1.

The crystalline quartz detector, attached to the other end of the polycrystalline quartz rod, was used in a feedback loop to stabilize the amplitude of the excited periodic strains. The amplitude of the excited periodic strains was determined by using the calibration procedure, in which the SMFMR of the polycrystalline nickel tape was measured. The ME constant of the polycrystalline nickel is known ( $b_1 = b_2 = 8.16 \times 10^7 \text{ erg/cm}^3$ ). Hence, performing two SMFMR experiments (in the external magnetic field parallel and perpendicular to the

TABLE I. The shifts of the FMR lines measured using the SMFMR technique for the  $\text{Co}_2\text{Fe}_x\text{Mn}_{1-x}\text{Si}$  ( $x = 0, 0.25, 0.4, 0.5, 0.6, 0.75,$  and  $1.0$ ) epitaxial magnetic layers, measured in-plane for the external magnetic field applied parallel to the  $[100]$  axis ( $\Delta H_{100}$ ) or  $[110]$  axis ( $\Delta H_{110}$ ), caused by the periodic strains  $\varepsilon_{11}$  and  $\varepsilon_{22}$  of the polycrystalline quartz rod, to which the thin films were glued.

$x$	$\Delta H_{100}$ (Oe)	$\varepsilon_{11}$ ( $10^{-6}$ )	$\varepsilon_{22}$ ( $10^{-5}$ )	$\Delta H_{110}$ (Oe)	$\varepsilon_{11}$ ( $10^{-6}$ )	$\varepsilon_{22}$ ( $10^{-5}$ )
0.0	$0.36 \pm 0.02$	$-3.0 \pm 0.2$	$1.61 \pm 0.05$	$0.45 \pm 0.02$	$-2.8 \pm 0.2$	$1.50 \pm 0.05$
0.25	$0.48 \pm 0.02$	$-2.6 \pm 0.2$	$1.43 \pm 0.05$	$0.45 \pm 0.02$	$-2.4 \pm 0.2$	$1.50 \pm 0.05$
0.4	$0.37 \pm 0.02$	$-2.8 \pm 0.2$	$1.52 \pm 0.05$	$0.83 \pm 0.02$	$-3.0 \pm 0.2$	$1.52 \pm 0.05$
0.5	$0.45 \pm 0.02$	$-3.1 \pm 0.2$	$1.58 \pm 0.05$	$1.14 \pm 0.02$	$-3.0 \pm 0.2$	$1.72 \pm 0.05$
0.6	$0.48 \pm 0.02$	$-2.8 \pm 0.2$	$1.70 \pm 0.05$	$1.01 \pm 0.02$	$-2.5 \pm 0.2$	$1.50 \pm 0.05$
0.75	$0.58 \pm 0.02$	$-3.0 \pm 0.2$	$1.65 \pm 0.05$	$1.22 \pm 0.02$	$-2.6 \pm 0.2$	$1.56 \pm 0.05$
1.0	$0.45 \pm 0.02$	$-2.7 \pm 0.2$	$1.57 \pm 0.05$	$1.53 \pm 0.02$	$-2.8 \pm 0.2$	$1.60 \pm 0.05$

nickel tape surface) enables determination of the amplitudes of the two periodic strain components  $\varepsilon_{11}$  and  $\varepsilon_{22}$ , i.e., in the direction perpendicular and parallel to the rod, respectively. Typical amplitudes of the periodic strain were about  $\varepsilon_{11} = 2.8 \times 10^{-6}$  and  $\varepsilon_{22} = 1.6 \times 10^{-5}$  (the shear strain  $\varepsilon_{12}$  in such experimental configuration is negligible). The calibration procedure was repeated for each experiment in order to increase the accuracy of the ME constants determination (see Table I).

In the SMFMR experiments, we determined the periodic shift of the FMR resonance line caused by the periodic strain. Figure 2 shows that the periodic shift of the resonance curve leads to periodic modulation of the absorbed power of the microwaves, and thus it is equivalent to the modulation of the external magnetic field. Hence, by comparison of the amplitudes of two FMR signals, one of which is modulated by the periodic strain and the second one by the magnetic field with known amplitude, the periodic shift of the FMR can be determined. If we denote the amplitude of the FMR line modulated by the strain as  $I_s$  and the amplitude of the FMR line modulated by magnetic field as  $I_m$ . The shift of the resonance line caused by the strain can then be calculated as  $\Delta H = (I_s/I_m)m_0$ , where  $m_0$  is the amplitude of the magnetic-field modulation [14]. The shift of the FMR resonance line is related to the ME effect. Thus using an appropriate model enables calculation of the ME constants.

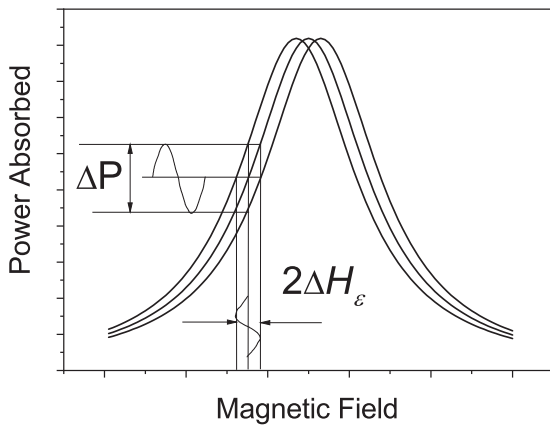


FIG. 2. The periodic shift of the resonance curve results in the modulation of an absorbed power  $\Delta P$ , giving an effect equivalent to the modulation of the external magnetic field with the amplitude  $\Delta H_\varepsilon$ .

We have performed SMFMR experiments for two sample orientations, both with the external magnetic field parallel to the surface of the film, but parallel to the  $[100]$  or  $[110]$  crystallographic axes of the epitaxially grown  $\text{Co}_2\text{Fe}_x\text{Mn}_{1-x}\text{Si}$  magnetic layer, respectively. The external magnetic field was perpendicular to the quartz rod, to which the investigated samples were glued (see Fig. 1). Such experimental arrangement enables determination of two cubic ME constants (see Sec. IV for a description and their application).

The maximal magnetic field induction attainable in our SMFMR system is about 1 tesla. To study the perpendicular MC anisotropy, additional FMR experiments using the X-band Bruker EMX spectrometer, with a maximal magnetic-field induction attainable of about 1.8 tesla, were performed. This spectrometer was also used to obtain the whole angular dependence of the resonance field.

To estimate the influence of the inhomogeneous broadening on the widths of the FMR lines, broadband FMR studies were performed, in the range of frequencies from 4 to 18 GHz. The investigated sample was put on the surface of the microstrip line, connected to a vector network analyzer (VNA).

### III. EXPERIMENTAL RESULTS

The FMR and SMFMR spectra of all investigated samples, for the external magnetic field applied in-plane of the sample and parallel to the  $[100]$  or  $[110]$  crystallographic axis of the epitaxial magnetic layer are shown in Figs. 3(a) and 3(b), respectively. The corresponding curves presented in Figs. 3(a) and 3(b) were registered in the same spectrometer and at the same conditions (sample orientation, microwave power, etc.) with the only difference that the magnetic modulation was changed by the strain modulation. For most samples (except that with  $x = 1.0$ ) resonance fields measured in the  $[110]$  direction are lower than those in the  $[100]$  direction, which means that the  $[110]$  direction is an easy axis of magnetization. Some of the FMR lines have the complex structure, which is probably connected with the mosaic structure of the epitaxial magnetic layers. The mosaic structure of the  $\text{Co}_2\text{Fe}_{0.4}\text{Mn}_{0.6}\text{Si}$  layer was detected by the x-ray studies in our previous investigations [8]. Heterogeneous structure of the magnetic layer may cause that the resonance conditions in different areas of the sample are different leading to a split of the FMR line. However, it is only one possible reason for splitting the FMR line, and to explain the nature of the complex structure of the FMR lines further investigations are

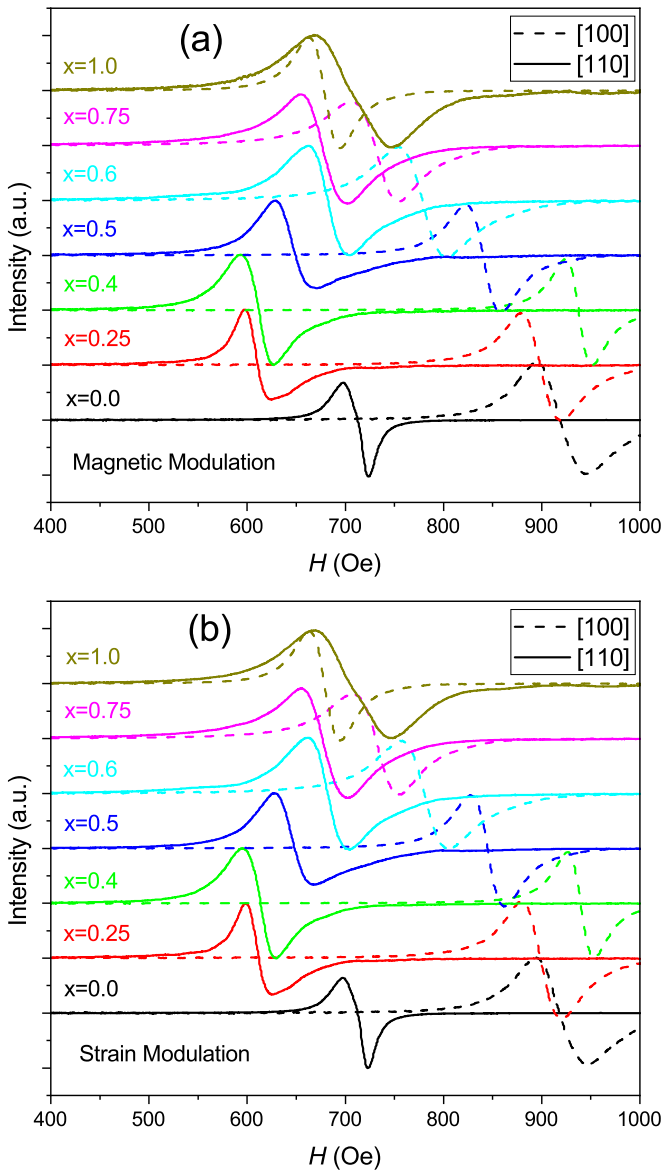


FIG. 3. The in-plane (a) FMR and (b) SMFMR spectra for the  $\text{Co}_2\text{Fe}_x\text{Mn}_{1-x}\text{Si}$  ( $x = 0, 0.25, 0.4, 0.5, 0.6, 0.75$ , and  $1.0$ ) epitaxial magnetic layers measured at the same conditions at the frequency of  $9.2$  GHz with the external magnetic field oriented along the  $[100]$  and  $[110]$  crystallographic axes, respectively.

necessary. Another reason of splitting the FMR line may be the excitation of different magnetostatic modes, the spin-wave resonance or angular properties of domain structure [21]. Both FMR and SMFMR spectra had the same shapes and differed only with amplitudes. In Fig. 3 the FMR and SMFMR spectra with normalized amplitudes are presented. The difference between the resonance field in the  $[110]$  and  $[100]$  applied magnetic-field directions is the largest for the sample with  $x = 0.4$ . For the sample with  $x = 1.0$  (no Mn) the resonance field measured in the  $[100]$  direction is slightly lower than that in  $[110]$  direction, which means that, for this composition, the easy magnetization axis changes from  $[110]$  to  $[100]$ . Figure 4 shows the angular dependence of the in-plane resonance field for the samples studied in the experiments. It

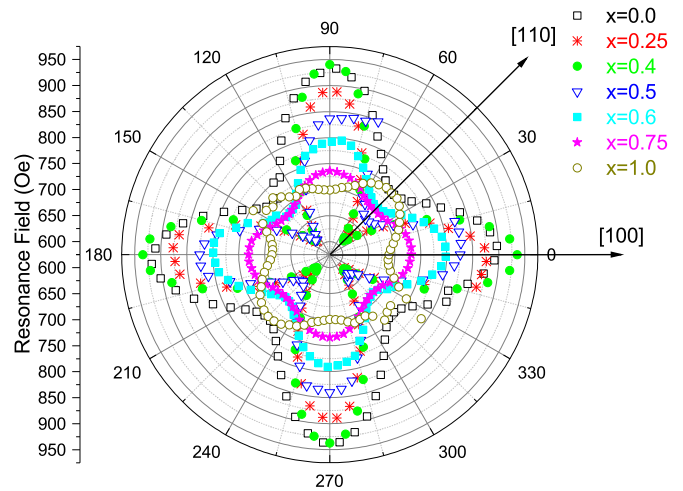


FIG. 4. The angular dependence of the in-plane FMR ( $9.38$  GHz) resonance field for the  $\text{Co}_2\text{Fe}_x\text{Mn}_{1-x}\text{Si}$  ( $x = 0, 0.25, 0.4, 0.5, 0.6, 0.75$ , and  $1.0$ ) epitaxial magnetic layers. The directions corresponding the  $[100]$  and  $[110]$  axes of the epitaxial magnetic layer are also shown.

is clearly seen that, for all samples, the fourfold in-plane anisotropy is dominating. The out-of-plane, i.e., with the external magnetic field applied perpendicularly to the film, FMR spectra (with normalized amplitudes) are shown in Fig. 5. Except of the slightly lower value of the perpendicular resonance

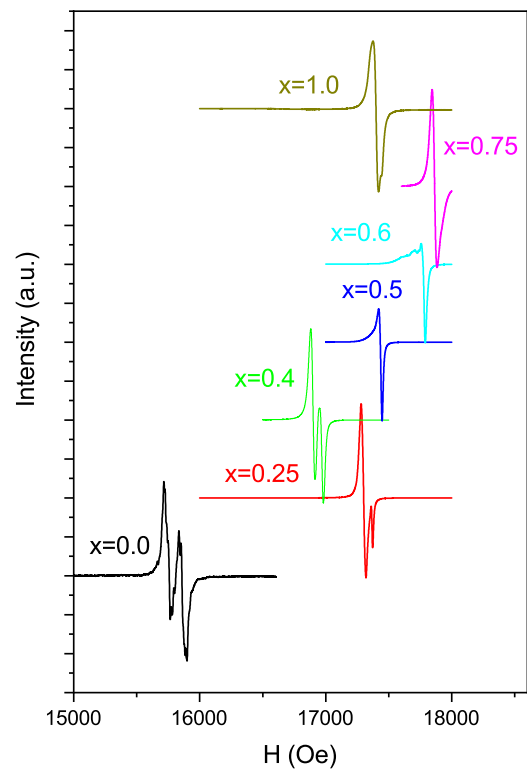


FIG. 5. The out-of-plane (with the external magnetic field applied perpendicularly to the film) FMR ( $9.38$  GHz) spectra for the  $\text{Co}_2\text{Fe}_x\text{Mn}_{1-x}\text{Si}$  ( $x = 0, 0.25, 0.4, 0.5, 0.6, 0.75$ , and  $1.0$ ) epitaxial films.

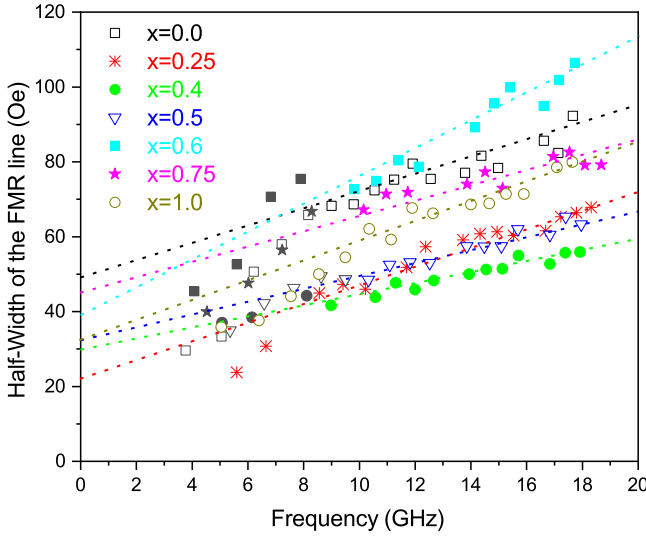


FIG. 6. The frequency dependence of the half width of the FMR lines taken for all studied  $\text{Co}_2\text{Fe}_x\text{Mn}_{1-x}\text{Si}$  magnetic layers, obtained using the VNA technique. The external magnetic field was applied in the film plane along the direction parallel to the [100] axis of the magnetic layer. Dotted lines show the extrapolation of the linear fit of the experimental data in the range of 10–18 GHz.

field for the sample with  $x = 0$  (no Fe), no systematic changes of the perpendicular resonance field with sample composition were observed. The complex structure of the lines is most probably connected with the mosaic structure of the magnetic layer.

The results of the SMFMR experiments are presented in Table I. This table presents the shifts of the FMR lines, caused by the periodic strains  $\varepsilon_{11}$  and  $\varepsilon_{22}$ , which were induced in a polycrystalline quartz rod and transferred to the thin film glued to its surface. The magnitudes of  $\varepsilon_{11}$  and  $\varepsilon_{22}$  for each experiment are also given in Table I. The opposite signs of  $\varepsilon_{11}$  and  $\varepsilon_{22}$  reflect the fact that stretching of the rod corresponds to a decrease of its diameter and vice versa.  $\Delta H_{100}$  and  $\Delta H_{110}$  denote the shifts of the resonance lines in the SMFMR experiments in which the [100] or [110] axes of the epitaxial layer were parallel to the external magnetic field and perpendicular to the rod, respectively. One can see that, with increasing Fe content, the changes of  $\Delta H_{100}$  are rather moderate. On the other hand, the  $\Delta H_{110}$  increases with increasing  $x$ . For the samples with  $x = 0.0$  and  $x = 0.25$  the magnitudes of  $\Delta H_{100}$  are very close to that of  $\Delta H_{110}$ , which is expected for the samples whose ME properties are isotropic. In the case of the sample with  $x = 1.0$ ,  $\Delta H_{110}$  is approximately three times larger than  $\Delta H_{100}$ , which is evidence of the anisotropy of the ME properties.

Figure 6 shows the frequency dependence of the half width of the FMR lines of all the samples studied in our experiments, in the frequency range from about 4 GHz to about 18 GHz, using the VNA technique. The external magnetic field was applied in the plane of the film and parallel to the [100] axis of the magnetic layer. Despite the large scattering of experimental data, it can be seen that, for all samples, the linear extrapolation of the high frequency (10–18 GHz) dependence of the half width to zero frequency does not cross the Y axis

at 0 Oe. Moreover, for most of the samples, the slope of the experimental curve for the frequency range below 10 GHz is greater than for the frequency range above 10 GHz.

#### IV. THEORETICAL MODEL DESCRIPTION AND THEIR APPLICATION

In the obtained data analysis, we assumed that the density of the free energy of the thin magnetic layer in external magnetic field is described by the following formula:

$$F = - \sum_{i=1}^3 M_i H_i + 2\pi M_s^2 \alpha_3'^2 + E_{mc} + E_{el} + E_{me}. \quad (1)$$

The first term in Eq. (1) is the density of Zeeman energy.  $M_i$  and  $H_i$  are the components of the magnetization and external magnetic-field intensity, respectively. The second term is a density of demagnetizing energy.  $M_s$  is saturation magnetization and  $\alpha_3'$  is one of the direction cosines of the magnetization. The prime symbol here, as well as in the next formulas, means that the coordinate system is associated with the sample (the symbols without primes means that the coordinate system is associated with the quartz rod). We assumed the 1, 2, and 3 axes of the Cartesian system associated with the sample to be parallel to the [100], [010], and [001] crystallographic axes, respectively (the [001] axis is perpendicular to the film).  $E_{mc}$  in Eq. (1) is the density of magnetocrystalline (MC) energy. This density of energy can be represented in the form [22]

$$E_{mc} = K_p(1 - \alpha_3'^2) + K_1(\alpha_1'^2\alpha_2'^2 + \alpha_2'^2\alpha_3'^2 + \alpha_1'^2\alpha_3'^2), \quad (2)$$

where  $K_p$  is the perpendicular MC constant, and  $K_1$  is the first cubic MC constant. In our analysis only the first cubic MC constant was considered.  $E_{el}$  in Eq. (1) is the density of elastic energy—for a cubic sample given by the formula [22] [see Eq. (43) in Ref. [22]] and note the difference in definitions of  $e_{ij}$  and  $\varepsilon_{ij}$ ; see Eqs. (31) and (32) in Ref. [22]]

$$E_{el} = \frac{1}{2}c_{11}(\varepsilon_{11}'^2 + \varepsilon_{22}'^2 + \varepsilon_{33}'^2) + c_{12}(\varepsilon_{11}'\varepsilon_{22}' + \varepsilon_{22}'\varepsilon_{33}' + \varepsilon_{11}'\varepsilon_{33}') + 2c_{44}(\varepsilon_{12}'^2 + \varepsilon_{23}'^2 + \varepsilon_{13}'^2), \quad (3)$$

where  $c_{ij}$  are elastic constants, and  $\varepsilon'_{ij}$  strain components (in the coordinate system associated with the sample). The last term in Eq. (1) is the density of ME energy. We assumed the density of ME energy of a cubic sample to be expressed by the formula [14]

$$E_{me} = b_1(\alpha_1'^2\varepsilon'_{11} + \alpha_2'^2\varepsilon'_{22} + \alpha_3'^2\varepsilon'_{33}) + 2b_2(\alpha_1'\alpha_2'\varepsilon'_{12} + \alpha_2'\alpha_3'\varepsilon'_{23} + \alpha_1'\alpha_3'\varepsilon'_{13}), \quad (4)$$

where  $b_1$  and  $b_2$  are the two cubic ME constants. When the external magnetic field was in-plane of the film and parallel the [100] crystallographic axis of the sample, the coordinate system associated with the sample coincided with that of the quartz rod. Additionally, we assumed the strain of the rod to be fully transferred into the sample. Hence,  $\varepsilon'_{11} = \varepsilon_{11}$ ,  $\varepsilon'_{22} = \varepsilon_{22}$ ,  $\varepsilon'_{12} = \varepsilon_{12} = 0$ . The other strain components ( $\varepsilon'_{33}$ ,  $\varepsilon'_{13}$ ,  $\varepsilon'_{23}$ ) were calculated by minimizing the sum of ME ( $E_{me}$ ) and elastic ( $E_{el}$ ) energy.

When the external magnetic field was applied in the film plane but parallel to the [110] axis of the magnetic layer, the coordinate system associated with the sample was rotated with respect to the system associated with the quartz rod around the [001] axis by 45 degrees. In this case  $\varepsilon'_{11} = \varepsilon'_{22} = \frac{1}{2}(\varepsilon_{11} + \varepsilon_{22})$  and  $\varepsilon_{12} = \frac{1}{2}(\varepsilon_{11} - \varepsilon_{22})$ .

To obtain the resonance conditions, it is convenient to change the direction cosines into the angles of the polar system ( $\theta$  and  $\varphi$ ) according to formulas  $\alpha_1 = \sin(\theta) \cos(\varphi)$ ,  $\alpha_2 = \sin(\theta) \sin(\varphi)$ , and  $\alpha_3 = \cos(\theta)$ . The resonance conditions can be next found by using the equations [23]

$$\frac{\partial F}{\partial \theta} = \frac{\partial F}{\partial \varphi} = 0 \quad (5)$$

and

$$\left(\frac{\omega}{\gamma}\right)^2 = \frac{1}{M_s^2 \sin^2 \theta} \left[ \left(\frac{\partial^2 F}{\partial \theta^2}\right) \left(\frac{\partial^2 F}{\partial \varphi^2}\right) - \left(\frac{\partial^2 F}{\partial \theta \partial \varphi}\right)^2 \right], \quad (6)$$

where  $\omega$  is the angular frequency and  $\gamma$  is the gyromagnetic ratio.

From Eq. (6), it is clearly seen that, in the calculation of the resonance conditions, only the terms of the density of the free energy which are angular dependent are important. The angular dependence of the contribution to the free energy of the perpendicular MC anisotropy [see term proportional to  $K_p$  in Eq. (2)] is the same as of the demagnetizing energy, i.e., both contributions are proportional to  $\alpha_3'^2$  or  $[\cos(\theta)]^2$ . For this reason it is convenient to introduce a new parameter called effective magnetization:

$$M_{\text{eff}} = M_s - \frac{K_p}{2\pi M_s}. \quad (7)$$

The contributions of both terms to the density of the free energy can then be combined into one segment:  $2\pi M_s M_{\text{eff}} \alpha_3'^2$ , which simplifies further calculations. One can see also that, in order to determine the  $K_p$  parameter from FMR experiments, knowledge of  $M_s$  is necessary. If one neglects the ME energy, uses Eqs. (1), (2), (5), (6), and (7), and considers the three sample orientations studied in our FMR experiments, one can find the following three resonance conditions:

$$\left(\frac{\omega}{\gamma}\right)^2 = \frac{1}{M_s^2} (2K_1 + H_{100} M_s) [2K_1 + M_s (H_{100} + 4\pi M_{\text{eff}})], \quad (8)$$

$$\left(\frac{\omega}{\gamma}\right)^2 = \frac{1}{M_s^2} (-2K_1 + H_{110} M_s) [K_1 + M_s (H_{110} + 4\pi M_{\text{eff}})], \quad (9)$$

$$\left(\frac{\omega}{\gamma}\right)^2 = \frac{1}{M_s^2} [2K_1 + M_s (H_{001} - 4\pi M_{\text{eff}})], \quad (10)$$

where  $H_{100}$ ,  $H_{110}$ , and  $H_{001}$  are the FMR resonance fields measured when the external magnetic field is parallel to the [100], [110], or [001] (i.e., perpendicular to the film), respectively. Using Eqs. (8)–(10), Eq. (7), and our experimental data, we could determine three parameters:  $K_1$ ,  $K_p$ , and the  $g$  factor, which is correlated with  $\gamma$  ( $\gamma = 2\pi g \mu_B / h$ , where  $\mu_B$  is Bohr magneton and  $h$  is Planck's constant). The values of saturation magnetization, which were used in our calculations, were

TABLE II. Saturation magnetization of the  $\text{Co}_2\text{Fe}_x\text{Mn}_{1-x}\text{Si}$  films studied in experiments.

$x$	0.0	0.25	0.4	0.5	0.6	0.75	1.0
$M_s$ (emu/cm <sup>3</sup> )	747	817	849	852	954	966	872

taken from Ref. [20], and they are also presented in Table II. A slight deviation from the linear dependence of magnetization on  $x$  for the samples with highest  $x$  is probably connected with the changes of the chemical ordering [see Fig. 2(s) in Ref. [20]].

The estimated  $g$  factors of all the samples were in the range of 2.0–2.1. The changes of the first cubic MC constant with the changes of magnetic layer composition are shown in Fig. 7.

Figure 7 presents also the changes of the resonance fields  $H_{100}$  and  $H_{110}$  as a function of sample composition. As might be expected, the largest difference between  $H_{100}$  and  $H_{110}$  corresponds to the largest magnitude of the cubic anisotropy constant (about  $-7.3 \times 10^4$  erg/cm<sup>3</sup>). According to the definition of  $K_1$  in Eq. (2) for all the samples except that with  $x = 1.0$ , the values of  $K_1$  are negative, and a pronounced minimum (maximum of the absolute value) at  $x = 0.4$  is observed.

The changes of the perpendicular MC anisotropy constant ( $K_p$ ) with the changes of magnetic layer composition are shown in Fig. 8.

According to the definition in Eq. (2), the perpendicular MC anisotropy constant is negative for all the samples investigated, which means that for all the samples the perpendicular MC anisotropy energy has a maximum when the direction of magnetization is perpendicular to the film. The magnitude of  $K_p$  is large—of the order of  $10^6$  erg/cm<sup>3</sup>. For most samples, no systematic changes of  $K_p$  with sample composition were observed (the magnitude is in the range from  $1.1 \times 10^6$  erg/cm<sup>3</sup>

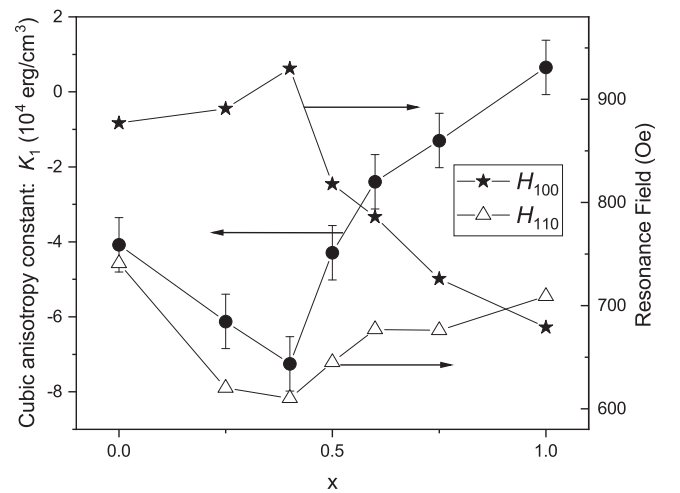


FIG. 7. The first cubic magnetocrystalline anisotropy constant  $K_1$  as a function of Fe content (black circles) for the  $\text{Co}_2\text{Fe}_x\text{Mn}_{1-x}\text{Si}$  magnetic layers studied in the experiments. The magnitudes of the resonance fields measured for the external magnetic field applied in the film plane and parallel to the [100] (stars) or [110] (triangles) crystallographic axis are also shown.

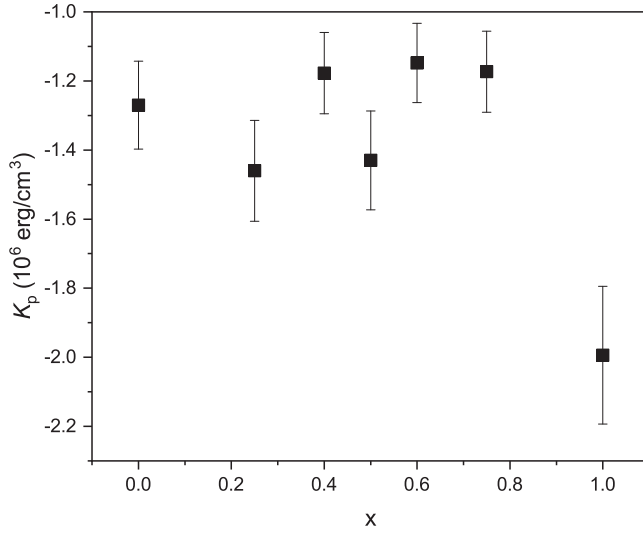


FIG. 8. The changes of the perpendicular magnetocrystalline anisotropy constant  $K_p$  as a function of the Fe content,  $x$ , in the  $\text{Co}_2\text{Fe}_x\text{Mn}_{1-x}\text{Si}$  magnetic layers.

to  $1.5 \times 10^6$  erg/cm<sup>3</sup>), a slightly higher magnitude of  $K_p$  ( $2 \times 10^6$  erg/cm<sup>3</sup>) was found for the sample with  $x = 1$ .

Now let us consider the influence of the periodic strain on resonance conditions. In this situation, the ME energy ( $E_{\text{me}}$ ) in Eq. (1) must be also taken into account. As the result of the ME effect, the periodic strain of the sample leads to a periodic shift of the resonance line, which is registered in our SMFMR experiments (see Table I). The shifts of the resonance lines  $\Delta H_{100}$  and  $\Delta H_{110}$  can be calculated by subtraction of the resonance field in the strained (i.e., with  $\varepsilon_{11} \neq 0$  and  $\varepsilon_{22} \neq 0$ ) and unstrained (i.e., with  $\varepsilon_{11} = 0$  and  $\varepsilon_{22} = 0$ ) conditions. If one takes into account only the linear terms with  $\Delta H_{100}$  or  $\Delta H_{110}$  the following formulas can be found:

$$\Delta H_{100} = \frac{A_{11}(H_{100} + H_k + 4\pi M_{\text{eff}}) - A_{12}(H_{100} + H_k)}{2H_{100} + 2H_k + 4\pi M_{\text{eff}}}, \quad (11)$$

$$\Delta H_{110} = \frac{A_{21}(\frac{3}{2}H_{110} + 4\pi M_{\text{eff}}) - C_2(H_{110} - H_k)}{2H_{110} - \frac{1}{2}H_k + 4\pi M_{\text{eff}}}, \quad (12)$$

where  $A_{11} = -\frac{2b_1}{M_s}(\varepsilon_{22} - \varepsilon_{11})$ ,  $A_{12} = -\frac{2b_1}{M_s}[\varepsilon_{11} + \frac{c_{12}}{c_{11}}(\varepsilon_{11} + \varepsilon_{22})]$ ,  $A_{21} = -\frac{2b_2}{M_s}(\varepsilon_{22} - \varepsilon_{11})$ ,  $C_2 = -\frac{2b_1}{M_s}(\frac{1}{2} + \frac{c_{12}}{c_{11}})(\varepsilon_{11} + \varepsilon_{22})$ , and  $H_k = \frac{2K_1}{M_s}$  is the anisotropy field.

Solving the set of equations (11) and (12) enables a determination of the two ME constants  $b_1$  and  $b_2$  for each sample. The calculated ME constants as a function of the Fe content in the  $\text{Co}_2\text{Fe}_x\text{Mn}_{1-x}\text{Si}$  magnetic layer,  $x$ , are presented in Fig. 9.

The two ME constants  $b_1$  and  $b_2$  defined by Eq. (4) are both negative for all the samples studied in our experiments. The negative values of magnetoelastic constants correspond to positive values of longitudinal magnetostriction [see Eqs. (13) and (14) below]. The magnitude of the  $b_1$  constant only slightly changes with magnetic layer composition and its magnitude is about  $1 \times 10^7$  erg/cm<sup>3</sup>. Approximately the same magnitude corresponds to the  $b_2$  constants for the samples with  $x = 0$  and  $x = 0.25$ , which means that ME properties

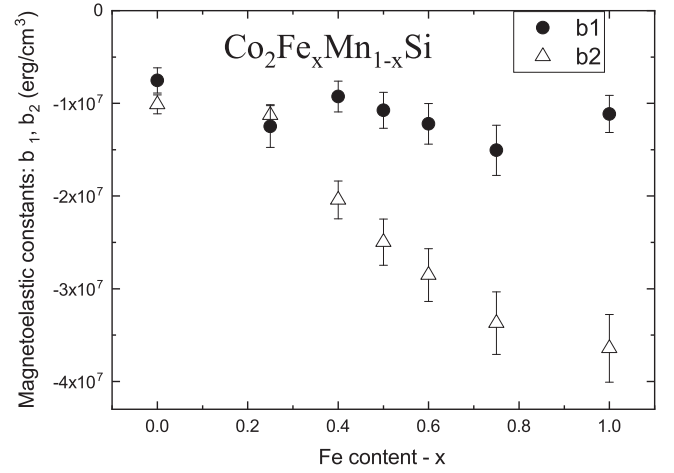


FIG. 9. Two magnetoelastic constants  $b_1$  and  $b_2$  for the series of the  $\text{Co}_2\text{Fe}_x\text{Mn}_{1-x}\text{Si}$  epitaxial magnetic layers with different Fe content  $x$ .

of these two samples may be, to a good approximation, considered as isotropic. On the other hand, for the samples with  $x > 0.25$  the systematic increase of the  $b_2$  constant with increasing Fe content was observed, reaching the magnitude of almost  $4 \times 10^7$  erg/cm<sup>3</sup> for the sample with  $x = 1.0$ .

The knowledge of all ME and elastic constants enables calculation of the saturation magnetostriction. However, the procedure presented below refers only to bulk materials, which are not anchored to a substrate. In magnetic thin films, which are deposited on a relatively thick substrate, the actual magnetostriction, i.e., the changes of the sample dimensions in external magnetic field, is usually very small. We present here this procedure for easier comparison of our results with other studies, in which instead of ME constants the magnetostriction coefficients are presented. By minimizing the sum of elastic [Eq. (3)] and ME [Eq. (4)] energies with respect to all strain components, the whole strain tensor can be obtained. The components of the strain tensor depend on the orientation of the sample magnetization (i.e., on  $\alpha'_i$  or on  $\theta$  and  $\varphi$ ). The saturation magnetostriction is a difference between chosen sample dimension in a magnetized and demagnetized state. To calculate the strain tensor in a demagnetized state, the strain components must be averaged over the full solid angle. We present here the results of the calculations of the longitudinal magnetostriction, i.e., when the changes of the sample dimensions are measured along the direction of the applied external magnetic field. It can be found that, for the [100] or [111] direction, the saturation longitudinal magnetostriction is given by the formulas

$$\lambda_{100} = -\frac{2b_1}{3(c_{11} - c_{12})}, \quad (13)$$

$$\lambda_{111} = -\frac{2b_2}{c_{44}}. \quad (14)$$

These two magnetostriction constants are most often presented for the samples with cubic symmetry. To calculate the magnetostriction constants, the elastic constants are also necessary. The elastic constants for all magnetic layer compositions studied here were not available in the literature. For

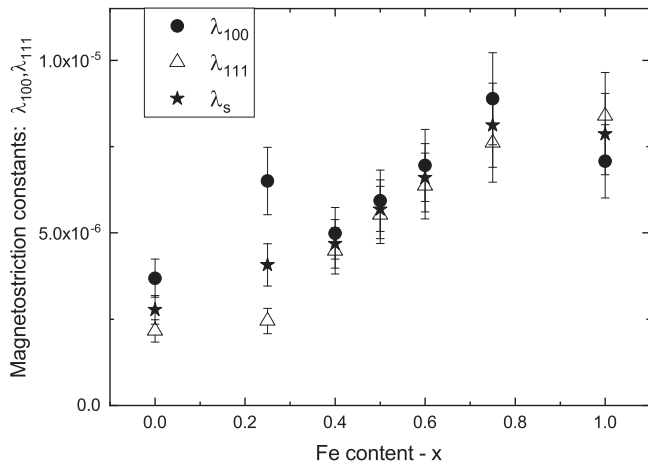


FIG. 10. The calculated  $\lambda_{100}$ ,  $\lambda_{111}$ , and averaged polycrystalline  $\lambda_s$  magnetostriction constants of the  $\text{Co}_2\text{Fe}_x\text{Mn}_{1-x}\text{Si}$  magnetic layers as a function of the Fe content  $x$ .

this reason, we took from Ref. [24]  $c_{11}(x=0) = 310.5$  GPa,  $c_{11}(x=1) = 273.6$  GPa,  $c_{12}(x=0) = 174.2$  GPa,  $c_{12}(x=1) = 168.5$  GPa,  $c_{44}(x=0) = 156.9$  GPa,  $c_{44}(x=1) = 144.7$  GPa, and for other compositions ( $0 < x < 1$ )  $c_{11}$ ,  $c_{12}$ , and  $c_{44}$  were calculated using linear interpolation.

The calculated  $\lambda_{100}$  and  $\lambda_{111}$  constants as a function of magnetic layer composition are shown in Fig. 10. Figure 10 presents also the calculated averaged saturation magnetostriction  $\lambda_s = (2\lambda_{100} + 3\lambda_{111})/5$ , which is expected for cubic polycrystalline materials with randomly oriented grains.

As one can see in Eqs. (13) and (14) that  $\lambda_{100}$  and  $\lambda_{111}$  are proportional to the ME constants  $b_1$  and  $b_2$ , respectively. Hence, one could expect similar behavior of the magnetostriction constants as the ME ones. However, a relatively large magnitude of the  $c_{44}$  elastic constant in comparison with  $\frac{1}{2}(c_{11} - c_{12})$  [note that, for a sample whose elastic properties are isotropic,  $c_{44} = \frac{1}{2}(c_{11} - c_{12})$ ] reduces the magnitude of  $\lambda_{111}$ . As a result, for most samples investigated,  $\lambda_{100}$  and  $\lambda_{111}$  have similar magnitudes. The magnitudes of all magnetostriction constants are below  $1 \times 10^{-5}$ , and the general tendency of the magnetostriction constant increase with increasing the Fe content can be observed.

The total broadening of the FMR line,  $\Delta H_{\text{tot}}$ , can be considered as a superposition of homogeneous,  $\Delta H_{\text{hom}}$ , and inhomogeneous,  $\Delta H_{\text{inhom}}$ , broadenings. Above certain frequency, in our case above about 10 GHz (see Fig. 4), the frequency dependence of the half width of the FMR line is linear, and the slope of the line is proportional to the Gilbert damping factor. This linear frequency-dependent contribution to the FMR linewidth ( $\Delta H_{\text{hom}} = 4\pi\alpha f/\gamma$ , where  $f$  is the frequency and  $\alpha$  is Gilbert damping factor) is called homogeneous broadening. The other ones are generally called inhomogeneous. Different mechanisms can be responsible for inhomogeneous broadening of the FMR line. One of which is called two-magnon scattering mechanism. The contribution to the width of the FMR line connected to this mechanism first nonlinearly increases with frequency and then above certain frequency it saturates. The change of slopes of experimen-

TABLE III. The inhomogeneous broadening  $\Delta H_{\text{inhom}}$  of the FMR lines of samples with different compositions obtained by subtracting the homogeneous broadening from the curves presented in Fig. 6.

$x$	0.0	0.25	0.4	0.5	0.6	0.75	1.0
$\Delta H_{\text{inhom}}$ (Oe)	49	20	30	32	39	46	32

tal curves presented in Fig. 6 suggests that the two-magnon scattering mechanism plays an important role also for our samples.

Table III presents the changes of the inhomogeneous broadening of the FMR lines with the sample composition. The magnitudes of  $\Delta H_{\text{inhom}}$  were obtained by fitting the experimental data shown in Fig. 6 in the frequency range from 10 to 18 GHz using the formula  $\Delta H_{\text{tot}} = \Delta H_{\text{inhom}} + 4\pi\alpha f/\gamma$ .

The inhomogeneous broadening of the FMR line changes nonmonotonically with the Fe content  $x$ , revealing a minimum around  $x = 0.25$ .

## V. DISCUSSION

The properties of the half-metallic  $\text{Co}_2\text{Fe}_x\text{Mn}_{1-x}\text{Si}$  Heusler alloys depend on the number of valence electrons, which increases with increasing Fe content [2]. The saturation magnetization is expected to increase linearly with  $x$  according to the Slater-Pauling rule [25,26]. However, not all properties of this alloy depend linearly on  $x$ . The theoretical calculations of the density of states at the Fermi level  $D_F$  show [27] that it has a minimum around  $x = 0.4$ . Taking into account the Kambersky's spin-flip scattering model [28], which predicts the Gilbert damping factor to be proportional to  $D_F$ , the minimum of  $D_F$  at  $x = 0.4$  was correlated with the minimum of Gilbert damping factor, studied in this compound using the TRMOKE magnetometer [6].

Although the magnitude of the first cubic MC constant estimated from our experiments is rather moderate (of an order of  $10^4$  erg/cm<sup>3</sup>, see Fig. 7), its dependence on  $x$  is very similar to that of Gilbert damping factor—see Fig. 11. This suggests that also the cubic MC anisotropy of our compounds is governed by the electronic band structure, and in particular by  $D_F$ . However, to find the quantitative correlation between the band structure and the cubic MC anisotropy, further investigations are necessary. In Ref. [19] both ME and MC constants were calculated for  $\text{Co}_2$ -based  $\text{Co}_2X\text{Al}$  ( $X = \text{V}, \text{Ti}, \text{Cr}, \text{Mn}, \text{Fe}$ ) full Heusler compounds. It was found that the MC anisotropy is expected to be different for different  $X$ , in particular when Mn is replaced by Fe. For the  $\text{Co}_2\text{Fe}_x\text{Mn}_{1-x}\text{Si}$  compound, the changes of the MC anisotropy with changing the Fe content have not been studied so far.

Our present study, as well as previous results for the thin films of  $\text{Co}_2\text{Fe}_{0.4}\text{Mn}_{0.6}\text{Si}$  [7,8], reveals a large (of the order of  $10^6$  erg/cm<sup>3</sup>) negative perpendicular MC anisotropy constant, see Fig. 8. Actually, this anisotropy constant is of the same order of magnitude and only 3–5 times lower than the density of demagnetizing energy  $2\pi M_s^2$ , which for our samples changes from  $3.5 \times 10^6$  erg/cm<sup>3</sup> (for  $x = 0$ ) to  $5.9 \times 10^6$  erg/cm<sup>3</sup> (for  $x = 0.75$ ). The negative value of

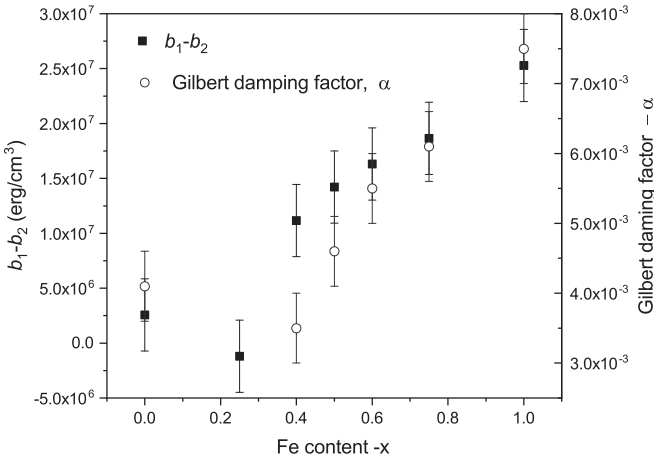


FIG. 11. Anisotropy of the magnetoelastic constants,  $b_1 - b_2$ , and Gilbert damping factor  $\alpha$  taken from Ref. [6] of the  $\text{Co}_2\text{Fe}_x\text{Mn}_{1-x}\text{Si}$  magnetic layers as a function of the Fe content  $x$ .

$K_p$  means that the in-plane orientation of magnetization becomes even more preferred. It was also found in Ref. [7] that, in the case of CFMS films, the magnitude of  $K_p$  increases with decreasing thickness of the magnetic layer, which may suggest the influence of the surface anisotropy [29]. The perpendicular MC anisotropy may also be a result of ME effect in combination with a tetragonal distortion induced by the mismatch between the magnetic layer and the substrate. Our recent results show that the magnitude of the tetragonal (i.e., with  $\varepsilon'_{11} = \varepsilon'_{22}$ ) distortion of  $\text{Co}_2\text{Fe}_{0.4}\text{Mn}_{0.6}\text{Si}$  films deposited on MgO also with 20 nm Cr buffer layer increases with decreasing thickness of the magnetic layer from about  $5 \times 10^{-4}$  to about  $5 \times 10^{-3}$  for the magnetic layer thickness of 50 and 15 nm, respectively. Such distortion, however, corresponds to the strain-induced MC anisotropy of about  $-2 \times 10^4$  erg/cm<sup>3</sup> and  $-1.4 \times 10^5$  erg/cm<sup>3</sup>, respectively, i.e., at least an order of magnitude smaller than that observed in our experiments.

In the case of nonmetallic materials or rare-earth metals, the two most important mechanisms of the magnetostriction are connected with the single-ion crystal-field effects or with the two-ion interactions [30]. These mechanisms, however, assume the localization of magnetic moments, and such an assumption in the case of half-metallic Heusler alloys may be doubtful. To calculate the MC anisotropy and magnetostriction of the  $\text{Co}_2\text{FeAl}$  and  $\text{Co}_2\text{MnAl}$  Heusler alloys, a first-principles calculation for the electronic structures was applied [19]. In our analysis, we used a phenomenological model which assumes that the density of ME energy is related to a change of the density of energy of MC anisotropy caused by a strain [see Eq. (4)]. This model is most often used to describe the magnetostriction of metallic alloys containing 3d metals. In this case, one can expect some correlation between the ME properties and MC anisotropy. In our case, both the cubic MC anisotropy and the ME constants change with magnetic layer composition. Although the character of the changes of the ME and cubic MC constants is slightly different, some similarities can be also found. For example, one can find the difference in the behavior of both ME and MC constants for the compositions with  $x$  below and above 0.4, respectively (compare Fig. 7

with Fig. 9). For compositions with  $x$  lower than 0.4, the two ME constants have similar magnitudes. For the composition with  $x = 0.4$  or higher, the magnitude of the  $b_2$  ME constant is higher than  $b_1$ , and the difference between both constants increases with increasing Fe content (see Fig. 9). The behavior of the cubic anisotropy constant below and above  $x = 0.4$  is also apparently different (see Fig. 7).

Figure 11 compares the anisotropy of the magnetoelastic properties, defined as the difference between the two cubic magnetoelastic constants, ( $b_1 - b_2$ ), with the Gilbert damping factor (taken from Ref. [6]) for different magnetic layer compositions. Although the minimum of the Gilbert damping dependence on  $x$  seems to be slightly shifted towards higher-Fe concentrations, both dependencies are quite similar. This fact suggests that, similarly to the Gilbert damping and the first cubic magnetocrystalline anisotropy constant (shown in Fig. 7), the anisotropy of the magnetoelastic properties is also correlated with the band structure of the investigated material.

An increase of saturation magnetization with  $x$  (see Table II) is accompanied by an increase of magnetostriction constants (Fig. 10). The magnitudes of the all estimated magnetostriction constants are relatively low, i.e., in the range from  $2 \times 10^{-6}$  to  $9 \times 10^{-6}$ . They are lower than the magnitudes of magnetostriction constants calculated in Ref. [19] for  $\text{Co}_2\text{FeAl}$  and  $\text{Co}_2\text{MnAl}$ , respectively. For  $\text{Co}_2\text{FeAl}$ , both magnetostriction constants were found to have similar magnitudes of about  $3 \times 10^{-5}$ , which is approximately four times larger value than in the case of our  $\text{Co}_2\text{FeSi}$ , for which  $\lambda_{100} = 7.0 \times 10^{-6}$  and  $\lambda_{111} = 8.4 \times 10^{-6}$ , respectively. Contrary to our results obtained for the  $\text{Co}_2\text{MnSi}$  sample, for which  $\lambda_{100} = 3.7 \times 10^{-6}$  and  $\lambda_{111} = 2.1 \times 10^{-6}$  have similar values, that calculated in Ref. [19] for  $\text{Co}_2\text{MnAl}$   $\lambda_{100} \approx 9 \times 10^{-5}$  and  $\lambda_{111} \approx -3 \times 10^{-5}$ , see Fig. 3(b) in Ref. [19]. They have also more than order of magnitude higher values than corresponding values estimated from our experiments for  $\text{Co}_2\text{MnSi}$ . On the other hand, the averaged for the polycrystalline  $\text{Co}_2\text{MnAl}$  magnetostriction constant  $\lambda_s = 1.8 \times 10^{-5}$  was estimated (in Ref. [19]) to be only slightly higher than that found experimentally in Ref. [31]:  $\lambda_s = 1.43 \times 10^{-5}$ . For the polycrystalline  $\text{Co}_2\text{FeAl}$  film, the saturation magnetostriction constant was found experimentally [32] to be  $\lambda_s = 1.4 \times 10^{-5}$ , i.e., approximately twofold lower than that estimated in Ref. [19] (about  $3 \times 10^{-5}$ ).

The correlation between the cubic MC anisotropy constant (Fig. 7) observed in our experiments and Gilbert damping (Fig. 11) may be understood as a result of the fact that both these parameters are related to the spin-orbit coupling strength. The results of our broadband FMR studies show also a strong inhomogeneous broadening of the FMR lines (Fig. 6 and Table III). In particular, an influence of the two-magnon scattering mechanisms was found. However, we cannot also exclude the contribution of other mechanisms (e.g., those connected with the mosaic structure of the films) responsible for inhomogeneous broadening. One of the broadening mechanisms can be also connected with the coexistence of both  $B2$  and  $L2_1$  ordering in our samples. The degree of order of the  $B2$  structure was found to slightly decrease with increasing iron content from about 0.8 for the sample with

$x = 0$  to about 0.6 for the sample with  $x = 1$ , respectively (see Fig. 2(s) in Ref. [20]). On the other hand, the changes of the total inhomogeneous broadening (Table III) are not monotonic, suggesting rather the correlation with the cubic anisotropy (Fig. 7) or magnetoelastic properties (Fig. 11). The interplay of large two-magnon FMR linewidth and low Gilbert damping in  $\text{Co}_2\text{MnSi}$ ,  $\text{Co}_2\text{MnAl}$ , and  $\text{Co}_2\text{FeAl}$  thin films was recently studied by Peria *et al.* in Ref. [33]. The two-magnon scattering was shown to be an extrinsic linewidth-broadening mechanism connected with the grain-like defects giving a random MC anisotropy field. However, the nature of these defects is not clarified yet. According to our results, an analysis of the inhomogeneities of magnetic properties in the Heusler alloy thin films should also take into account both the MC anisotropy and the anisotropy of ME properties, which are both changing with the sample composition. For practical applications both homogeneous, i.e., Gilbert damping, and inhomogeneous, e.g., two-magnon scattering, mechanisms are important. Unfortunately because of mosaic structure of the investigated samples, the measured angular dependencies of the widths of the FMR lines (taken at 9.38 GHz, not presented here) have very irregular shapes, which makes an analysis of the different contributions to the inhomogeneous broadening of the FMR line very difficult.

The results of all our up-to-date investigations of the Heusler alloy thin films reveal a presence of a large perpendicular MC anisotropy, described [according to the definition in Eq. (2)] by a negative anisotropy constant  $K_p$ . The nature of this anisotropy is not clarified yet and needs further investigations. All the thin films in the present study have the magnetic layer thickness of 30 nm. The influence of the magnetic layer thickness on the anisotropy of ME constants as well as on the cubic MC anisotropy will be a subject of further research. Also the influence of the chemical ordering on the

MC anisotropy and ME effects needs further investigations. Similar studies are still absent from the literature.

## VI. CONCLUSIONS

The magnitude (its absolute value) of the cubic magnetocrystalline anisotropy constant ( $K_1$ ) of the 30 nm  $\text{Co}_2\text{Fe}_x\text{Mn}_{1-x}\text{Si}$  films reveals a pronounced maximum at  $x = 0.4$  correlated with the changes in the density of states at the Fermi level for the minority-spin channel. For  $x = 0.4$  or higher the two cubic ME constants ( $b_1$  and  $b_2$ ) are clearly different, and the difference between them increases with increasing iron content. Hence, with increasing the Fe content the magnetoelastic properties of the  $\text{Co}_2\text{Fe}_x\text{Mn}_{1-x}\text{Si}$  films becomes more and more anisotropic. On the other hand, the anisotropy of the magnetostriction constants ( $\lambda_{100}$  and  $\lambda_{111}$ ) is rather moderate. Also the magnitudes of the estimated magnetostriction constants are relatively low. They increase with increasing the Fe content, and with increasing saturation magnetization, from about  $2 \times 10^{-6}$  to about  $9 \times 10^{-6}$ . All the investigated samples are characterized by large (of an order of  $10^6$  erg/cm<sup>3</sup>) negative perpendicular MC anisotropy constant. For this reason, the in-plane orientation of magnetization becomes even more preferred. Despite low values of the Gilbert damping factor, the widths of the FMR lines of all samples investigated reveal large inhomogeneous broadening related among others to the two-magnon scattering mechanism.

## ACKNOWLEDGMENTS

This work was supported by the National Science Centre of Poland, Project No. 2018/31/B/ST7/04006. The authors also thank K. Nesteruk for the construction of the system for strain modulation and R. Żuberek for fruitful discussions.

- 
- [1] Y. Sakuraba, T. Iwase, K. Saito, S. Mitani, and K. Takanashi, *Appl. Phys. Lett.* **94**, 012511 (2009).
  - [2] B. Balke, G. H. Fecher, H. C. Kandpal, C. Felser, K. Kobayashi, E. Ikenaga, J. J. Kim, and S. Ueda, *Phys. Rev. B* **74**, 104405 (2006).
  - [3] T. Yamamoto, T. Seki, and K. Takanashi, *Phys. Rev. B* **94**, 094419 (2016).
  - [4] D. Steil, S. Alebrand, T. Roth, M. Krauß, T. Kubota, M. Oogane, Y. Ando, H. C. Schneider, M. Aeschlimann, and M. Cinchetti, *Phys. Rev. Lett.* **105**, 217202 (2010).
  - [5] Ch. Guillemand, W. Zhang, G. Malinowski, C. de Melo, J. Gorchon, S. Petit-Watelot, J. Ghanbaja, S. Mangin, P. Le Fèvre, F. Bertran, and S. Andrieu, *Adv. Mater.* **32**, 1908357 (2020).
  - [6] S. Pan, T. Seki, K. Takanashi, and A. Barman, *Phys. Rev. B* **101**, 224412 (2020).
  - [7] O. M. Chumak, A. Nabiałek, R. Żuberek, I. Radelytskyi, T. Yamamoto, T. Seki, K. Takanashi, L. T. Baczewski, and H. Szymczak, *IEEE Trans. Magn.* **53**, 2501906 (2017).
  - [8] O. M. Chumak, A. Pacewicz, A. Lynnyk, B. Salski, T. Yamamoto, T. Seki, J. Z. Domagala, H. Głowski, K. Takanashi, L. T. Baczewski, H. Szymczak, and A. Nabiałek, *Sci. Rep.* **11**, 7608 (2021).
  - [9] A. Magni, G. Bertotti, I. D. Mayergoyz, and C. Serpico, *Phys. B (Amsterdam, Neth.)* **306**, 121 (2001).
  - [10] R. Bonin, M. L. Schneider, T. J. Silva, and J. P. Nibarger, *J. Appl. Phys.* **98**, 123904 (2005).
  - [11] S. Emori, B. A. Gray, H.-M. Jeon, J. Peoples, M. Schmitt, K. Mahalingam, M. Hill, M. E. McConney, M. T. Gray, U. S. Alaun, A. C. Bornstein, P. Shafer, A. T. N'Diaye, E. Arenhloz, G. Haugstad, K.-Y. Meng, F. Yang, D. Li, S Mahat, D. G. Cahill, P. Dhagat *et al.*, *Adv. Mater.* **29**, 1701130 (2017).
  - [12] E. du Termolet de Lacheisserie, *Magnetostriction: Theory and Application of Magneto-elasticity* (CRC Press, Boca Raton, 1993), pp. 319–337.
  - [13] J. C. M. Henning and J. H. den Boef, *Appl. Phys. (Berlin)* **16**, 353 (1978).
  - [14] K. Nesteruk, R. Żuberek, S. Piechota, M. W. Gutowski, and H. Szymczak, *Meas. Sci. Technol.* **25**, 075502 (2014).
  - [15] J. E. Goldman, *Phys. Rev.* **72**, 529 (1947).
  - [16] A. M. Severino and F. P. Missell, *J. Magn. Magn. Mater.* **68**, 291 (1987).

- [17] H. Ratajczak and I. Gościńska, *Phys. Status Solidi A* **152**, 523 (1995).
- [18] D. García, J. L. Munoz, F. J. Castano, C. Parados, A. Asenjo, J. M. Garcia, and M. Vazquez, *J. Appl. Phys.* **85**, 4809 (1999).
- [19] F. Mahfouzi, G. P. Carman, and N. Kioussis, *Phys. Rev. B* **102**, 094401 (2020).
- [20] See Supplemental Material of Ref. [6].
- [21] A. H. Morrish, *The Physical Principles of Magnetism* (IEEE Press, New York, 2001).
- [22] C. Kittel, *Introduction to Solid State Physics*, Seventh edition (Jonh Wiley & Sons, Inc., New York, Chichester, Brisbane, Toronto, Singapore, 1996).
- [23] H. Suhl, *Phys. Rev.* **97**, 555 (1955).
- [24] S.-C. Wu, G. H. Fecher, S. Shahab Naghavi, and C. Felser, *J. Appl. Phys.* **125**, 082523 (2019).
- [25] J. C. Slater, *Phys. Rev.* **49**, 931 (1936).
- [26] L. Pauling, *Phys. Rev.* **54**, 899 (1938).
- [27] M. Oogane, T. Kubota, Y. Kota, S. Mizukami, H. Naganuma, A. Sakuma, and Y. Ando, *Appl. Phys. Lett.* **96**, 252501 (2010).
- [28] V. Kamberský, *Can. J. Phys.* **48**, 2906 (1970).
- [29] L. Neel, *J. Phys. Radium* **15**, 225 (1954).
- [30] E. Callen, *J. Appl. Phys.* **39**, 519 (1968).
- [31] J. J. Qiu, G. C. Han, W. K. Yeo, P. Luo, Z. B. Guo, and T. Osipowicz, *J. Appl. Phys.* **103**, 07A903 (2008).
- [32] M. Gueye Jr., B. M. Wague, F. Zighem, M. Belmeguenai, M. S. Gabor, T. Petrisor, Jr., C. Tiusan, S. Merccone, and D. Faurie, *Appl. Phys. Lett.* **105**, 062409 (2014).
- [33] W. K. Peria, T. A. Peterson, A. P. McFadden, T. Qu, C. Liu, C. J. Palmstrøm, and P. A. Crowell, *Phys. Rev. B* **101**, 134430 (2020).